Automatic prostate cancer detection through DCE-MRI images: all you need is a good normalization

Guillaume Lemaître[a,b,*], Robert Martí[b], Fabrice Meriaudeau[a,c]

[a] *LE2I UMR6306, CNRS, Arts et Métiers, Univ. Bourgogne Franche-Comté, 12 rue de la Fonderie, 71200 Le Creusot, France*
[b] *ViCOROB, Universitat de Girona, Campus Montilivi, Edifici P4, 17071 Girona, Spain*
[c] *CISIR, Electrical & Electronic Engineering Department, Universiti Teknologi Petronas, 32610 Seri Iskandar, Perak, Malaysia*

Abstract

This template helps you to create a properly formatted LaTeX manuscript.

Keywords: DCE-MRI, prostate cancer, normalization, classification, quantification

1. Introduction

Prostate Cancer (PCa) is the second most frequently diagnosed men cancer, accounting for 899,000 cases leading to 258,100 deaths (Ferlay et al., 2010). As highlighted by the PI-RADS Steering Committee, the two main challenges to be addressed are (Weinreb et al., 2016): (i) the improvement of detecting clinically significant PCa and (ii) an increase of the confidence in benign or dormant cases, avoiding unnecessary invasive medical exams. In this regard, multiparametric Magnetic Resonance Imaging (MRI) (mpMRI) is frequently used to build robust Computer-Aided Detection and Diangosis (CAD) systems to detect, localize, and grade PCa. In general, CAD systems are based on mpMRI which combines several of the following modalities (Lemaître et al., 2015): T_2 Weighted (T_2-W)-MRI, Dynamic Contrast-Enhanced (DCE)-MRI, Apparent Diffusion Coefficient (ADC) maps, and Magnetic Resonance Spectroscopy Imaging (MRSI).

*Corresponding author.
Email address: g.lemaitre58@gmail.com (Guillaume Lemaître)

In DCE-MRI, a contrast media is injected intravenously and a set of images is acquired over time. Consequently, each voxel in the image is a dynamic signal which is related to the vascular properties of the tissue. In fact, these properties are automatically extracted using quantitative or semi-quantitative approaches (Lemaître et al., 2015).

The former group of approaches uses pharmacokinetic modelling based on a bicompartment model, namely Brix (Brix et al., 1991) and Tofts (Tofts et al., 1995) models. The parameters of the Brix model are found assuming a linear relationship between the media concentration and MRI signal intensity. This assumption has shown, however, to lead to inaccurate parameter calculation (Heilmann et al., 2006). In the contrary, Tofts model only requires a conversion from MRI signal intensity to concentration, which can become a non-linear relationship using specific equation of MRI sequences (e.g., FLASH sequence). Tofts modelling suffers, however, from an higher complexity (Gliozzi et al., 2011). The conversion using the non-linear approach requires to acquire a T_1 map which is not always possible during clinical examination. Furthermore, the parameter calculation require the Arterial Input Function (AIF) which is challenging to measure and can also lead to inaccurate estimation of the parameters.

The latter group of approaches are rather mathematical than pharmacokinetic modelling (Huisman et al., 2001; Gliozzi et al., 2011). These methods offer the advantages to not require any knowledge about the MRI sequence nor any conversion from signal intensity to concentration. However, the heuristic approach propose by Huisman et al. requires an estimate regarding the noise standard deviation of the signal as well as manual tuning.

Nevertheless, all presented methods suffer from two major drawbacks: (i) the inter-patient variability of the data lead to a variation of the parameters estimated and to poor classification performance while designing CAD systems, and (ii) only few parameters are used to characterize the dynamic signal implying that some information are discarded.

In this work, we propose a fully automatic normalization method for DCE-MRI that reduce the inter-patient variability of the data. Furthermore, we show

that using the full normalized signal lead to the best classification performance.

The paper is organized as follows: Section 2 outlines our normalization strategy (Section 2.1) as well as specificity regarding the state-of-the-art methods used for comparison (Section 2.2). The dataset, experiments, and results are reported in Section 3 while discussed in Section 4 followed by a concluding section.

2. Methods

2.1. Normalization of DCE-MRI images

2.2. Quantification of DCE-MRI

2.2.1. Brix and Hoffmann models

In the Brix model (Brix et al., 1991), the MRI signal intensity is assumed to be proportional to the media concentration. Therefore, the model is expressed as in Eq. (1):

$$s_n(t) = 1 + A\left[\frac{\exp(k_{el}t') - 1}{k_{ep}(k_{ep} - k_{el})}\exp(-k_{el}t) - \frac{\exp(k_{ep}t') - 1}{k_{el}(k_{ep} - k_{el})}\exp(-k_{ep}t)\right], \quad (1)$$

with

$$s_n(t) = \frac{s(t)}{S_0}, \quad (2)$$

where $s(t)$ and S_0 are the MRI signal intensity at time t and the average pre-contrast MRI signal intensity, respectively; A, k_{el}, and k_{ep} are a constant proportional to the transfer constant, the diffusion rate constant, and the rate constant, respectively. Additionally, during the injection time $0 \leqslant t \leqslant \tau$, $t' = t$ and afterwards while $t > \tau$, $t' = \tau$.

Following this model, Hoffmann et al. propose the following similar model as expressed in Eq. (3):

$$s_n(t) = 1 + \frac{A}{\tau}\left[\frac{k_{ep}\left(\exp(k_{el}t') - 1\right)}{k_{el}(k_{ep} - k_{el})}\exp(-k_{el}t) - \frac{\exp(k_{ep}t') - 1}{(k_{ep} - k_{el})}\exp(-k_{ep}t)\right]. \quad (3)$$

The parameters are estimated by fitting the model using non-linear least-squares optimization solved with Levenberg-Marcquardt.

2.2.2. Tofts model

The extended Tofts model is formulated as in Eq. (4):

$$C_t(t) = K_{trans} C_p(t) * \exp(-k_{ep} t) + v_p C_p(t), \tag{4}$$

where $*$ is the convolution operator; $C_t(t)$ and $C_p(t)$ is the concentration of contrast agent in the tissue and in the plasma, respectively; K_{trans}, k_{ep}, and v_p are the volume transfer constant, the diffusion rate constant, and the plasma volume fraction, respectively.

Therefore, Tofts model requires to: (i) detect candidate voxels from the femoral or iliac arteries and estimate a patient-based AIF signal, (ii) convert the MRI signal intensity (i.e., AIF and dynamic signal) to a concentration, and (iii) in the case of a population-based AIF, estimate an AIF signal.

Segmentation of artery voxels and patient-based AIF estimation The AIF signal from DCE-MRI can be manually estimated by selecting the most-enhanced voxels from the femoral or iliac arteries (Meng et al., 2010). Few methods have been proposed to address the automated extraction of AIF signal. Chen et al. filter successively the possible candidates (Chen et al., 2008): (i) dynamic signals with small peak are rejecting by thresholding, (ii) voxels with a small wash-in are rejected by thresholding, (iii) a blob detector is used and large enough regions are kept, and (iv) circular and cylindricality are used to reject the last false positive. Zhu et al. propose an iterative method selecting voxels which best fit a gamma variate function (Zhu et al., 2011). However, it requires to compute first and second derivatives as well as maximum curvature points. Shanbhag et al. propose a 4-steps algorithm (Shanbhag et al., 2012; Fennessy et al., 2015): (i) remove slices with artefacts and find the best slices based on intrinsic anatomic landmarks and enhancement characteristics, (ii) find the voxel

candidates using the maximum enhanced voxels and a multi-label maximum entropy based thresholding algorithm, (iii) excluding region next to the endorectal coil, and (iv) selecting the best 5 candidates which meet enhancement characteristics and that are correlated.

All the above methods are rather complex and thus we propose a method which is based on the following simple assumptions: (i) all possible AIF signal candidates should have a similar shape, (ii) an high enhancement, and (iii) the arteries should be almost round and within a size range. Therefore, each slice is clustered into regions using K-means clustering with $k = 6$. The cluster with the highest enhancement—i.e. corresponding to the 90^{th} percentile of the maximum of each dynamic signal—contain the arteries and is selected. Finally, regions with an eccentricity smaller than 0.5 and an area in the range of $[100, 400]$ voxels are kept. Additionally, to remove voxels contaminated by partial volume effect, only the 10% most enhanced voxels of the possible candidates are kept as proposed by (Schabel and Parker, 2008) and the average signal is computed. A summary of the different segmentation steps is presented in Fig. **??**.

Conversion of MRI signal intensity to concentration To estimate the free parameters of the Tofts model (see Eq. (4)), the concentration $C_t(t)$ and $C_p(t)$ need to be computed from the MRI signal intensity and the AIF signal, respectively. This conversion is based on the equation of the FLASH sequence—see Appendix A for details—and is formulated as in Eq. (5):

$$c(t) = \frac{1}{TR \cdot r_1} \ln\left(\frac{1 - \cos\alpha \cdot S^* \frac{s(t)}{S_0}}{1 - S^* \frac{s(t)}{S_0}}\right) - \frac{R_{10}}{r_1}, \tag{5}$$

with,

$$S^* = \frac{1 - \exp(-TR \cdot R_{10})}{1 - \cos\alpha \cdot \exp(-TR \cdot R_{10})}, \tag{6}$$

where $s(t)$ is the MRI signal, S_0 is the MRI signal prior to the injection of the contrast media, α is the flip angle, TR is the Repetition Time (TR), R_{10} is the pre-contrast tissue relaxation time also equal to $\frac{1}{T_{10}}$, r_1 is the relaxitivity coefficient of the contrast agent.

T_{10} can be estimated from the acquisition of a T_1 map. However, this modality was not part of the clinical trial in this research and the value of T_{10} was fixed to 1600 ms for both blood and prostate as stated in the literature (Fennessy et al., 2015; De Bazelaire et al., 2004; Carr and Carroll, 2011).

Estimation of population-based AIF While estimating the pharmacokinetic parameters from Tofts model, the AIF concentration $C_p(t)$ can be computed either from the patient or a population. We presented in the two previous sections the algorithms which allows to estimate the patient-based AIF concentration. To compare with the previous approach, we also computed a population-based AIF which will be also later used to compare the performance of both approaches. In that regard, the population-based AIF was estimated as in (Meng et al., 2010) by fitting the average patient-based AIFs to the model of Parker et al. (2006) which is formulated as in Eq. (7):

$$C_p(t) = \sum_{n=1}^{2} \frac{A_n}{\sigma_n \sqrt{2\pi}} \exp\left(\frac{-(t-T_n)^2}{2\sigma_n^2}\right) + \frac{\alpha \exp(-\beta t)}{1+\exp -s(t-\tau)}, \qquad (7)$$

where A_n, T_n, and σ_n are the scaling constants, centers, and widths of the n^{th} Gaussian, α and β are the amplitude and decay constant of the exponential; and s and τ are the width and center of the sigmoid function, respectively.

The parameters are estimated by fitting the model using non-linear least-squares optimization solved with Levenberg-Marcquardt.

2.2.3. PUN model

Gliozzi et al. show that Phenomenological Universalities (PUN) approach can be used for DCE-MRI analysis (Gliozzi et al., 2011). The model has been successfully used in a CAD system proposed by Giannini et al. (2015). This

model can be expressed as in Eq. (8):

$$s_n(t) = \exp\left[rt + \frac{1}{\beta}\left(a_0 - r\right)\left(\exp(\beta t) - 1\right)\right], \tag{8}$$

with

$$s_n(t) = \frac{s(t) - S_0}{S_0}, \tag{9}$$

where $s(t)$ and S_0 are the MRI signal intensity at time t and the average pre-contrast MRI signal intensity, respectively; r, a_0, and β are the free parameters of the model.

The parameters are estimated by fitting the model using non-linear least-squares optimization solved with Levenberg-Marcquardt.

2.2.4. Semi-quantitative analysis

The semi-quantitative analysis of the DCE-MRI is equivalent to extract curve characteristics directly from the signal without a strict theoretical pharmacokinetic meaning. In this work, we use the model presented by Huisman et al. (2001) which formulate the MRI signal as in Eq. (10):

$$s(t) = \begin{cases} S_0 & 0 \leqslant t \leqslant t_0 \\ S_M - (S_M - S_0)\exp\left(\frac{-(t-t_0)}{\tau}\right) & t_0 < t \leqslant t_0 + 2\tau \\ S_M - (S_M - S_0)\exp\left(\frac{-(t-t_0)}{\tau}\right) + w(t - t_0 + 2\tau) & t > t_0 + 2\tau \end{cases} \tag{10}$$

where $s(t)$ is the MRI signal intensity, S_0 is the pre-contrast signal intensity, t_0 is the time corresponding to the start of enhancement, S_M and τ is the maximum of the signal and the exponential time constant, and w is the slope of the linear part.

Huisman et al. argue that curve fitting via least-squares minimization using Nelder-Mead algorithm leads to inaccurate estimation of the free parameters: mainly the issue come from an incorrect estimation of the start of enhancement t_0 leading to incorrect estimation of the other parameters. Therefore, they

propose to: (i) estimate robustly t_0, (ii) estimate S_0 by averaging the samples between 0 and t_0 (ii) estimate w depending if the slope is significant or not, (iii) estimate S_M which should be the point at the intersection of the most probable slope line and the plateau.

Instead of these successive estimations, we propose a unified optimization in which t_0 is fixed since that this is a key parameter. Therefore, t_0 is robustly estimated from the AIF signal since that this is the most enhanced signal in which the start of enhancement is easily identifiable. The AIF signal is computed as in Section 2.2.2. t_0 is estimated by finding the maximum in the beginning of the first derivative of the MRI signal. Then, the function in Eq. (10) is fitted using non-linear least squares with Trust Region Reflective algorithm. Furthermore, the parameters τ and S_M are bounded during the optimization to ensure robust estimations.

From Eq. (10), the following features are extracted: (i) the wash-in corresponding to the slope between t_0 and $t_0 + 2\tau$, (ii) the wash-out corresponding to the parameter w, (iii) the area under the curve between t_0 and the end of the signal, (iv) the exponential time constant τ, and (v) the relative enhancement $S_M - S_0$.

3. Experiments and results

4. Discussions

5. Conclusions and future works

Appendix A. Conversion from FLASH signal to media concentration

In this appendix, we show the demonstration used to extract the agent concentration from the MRI signal.

The signal equation in FLASH sequence (Haase et al., 1986) is defined as:

$$s(t) = S_{eq} \sin\alpha \cdot \frac{1 - \exp\left(-TR\left(R_{10} + r_1 c(t)\right)\right)}{1 - \cos\alpha \cdot \exp\left(-TR\left(R_{10} + r_1 c(t)\right)\right)}, \tag{A.1}$$

Table 1: AUC of the individual features for each method.

Features	Un-normalized data	Normalized data
Brix model		
A		
k_{el}		
k_{ep}		
Hoffmann model		
A		
k_{el}		
k_{ep}		
Tofts model with population AIF		
K_{trans}		
v_p		
k_{ep}		
Tofts model with patient AIF		
K_{trans}		
v_p		
k_{ep}		
PUN model		
a_0		
r		
β		
Semi-quantitative analysis		
wash-in		
wash-out		
IAUC		
τ		
$S_M - S_0$		

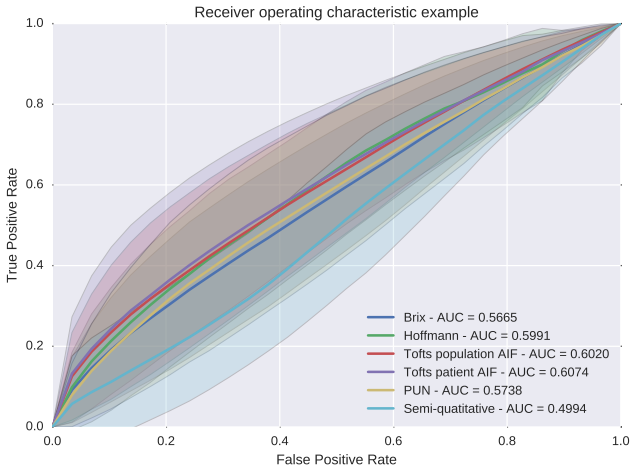

Figure 1: ROC analysis using a RF classifier for the different quantification methods without data normalization.

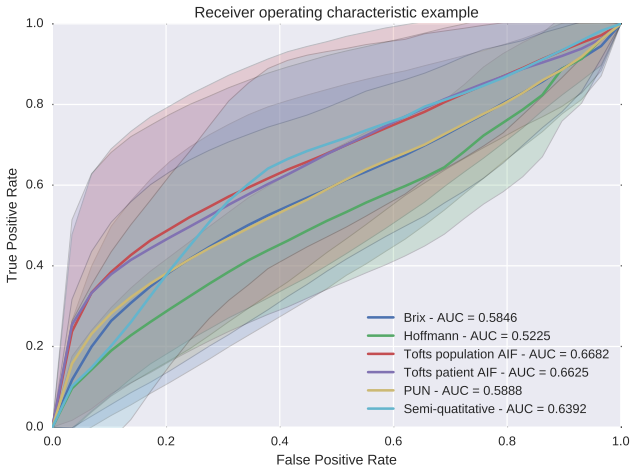

Figure 2: ROC analysis using a NB classifier for the different quantification methods without data normalization.

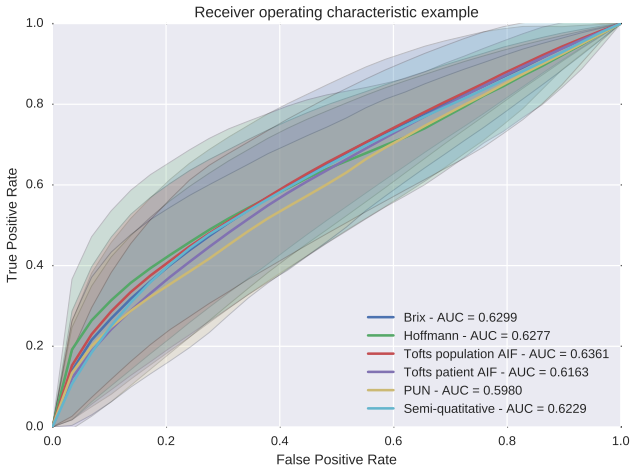

Figure 3: ROC analysis using a RF classifier for the different quantification methods with data normalization.

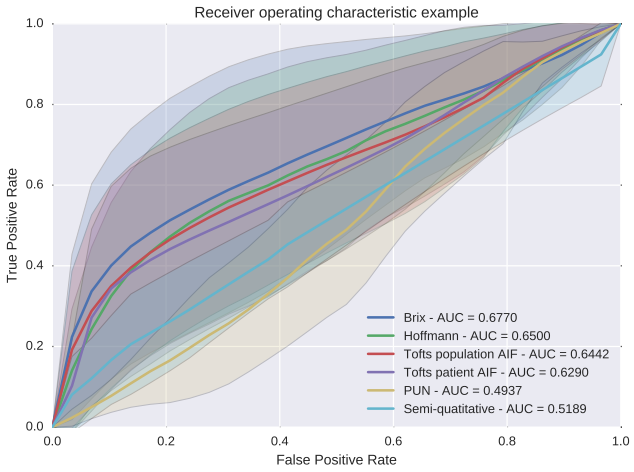

Figure 4: ROC analysis using a NB classifier for the different quantification methods with data normalization.

where $s(t)$ is the MRI signal, S_{eq} is the maximum signal amplitude of the spoiled gradient at the Echo Time (TE) which is proportional to the Proton Density (PD), α is the flip angle, TR is the Repetition Time (TR), R_{10} is the pre-contrast tissue relaxation time also equal to $\frac{1}{T_{10}}$, r_1 is the relaxitivity coefficient of the contrast agent, and $c(t)$ is the media concentration.

Therefore, the pre-contrast signal prior to bolus injection of the media is defined as:

$$S_0 = S_{eq} \sin\alpha \cdot \frac{1 - \exp\left(-TR \cdot R_{10}\right)}{1 - \cos\alpha \cdot \exp\left(-TR \cdot R_{10}\right)}. \tag{A.2}$$

To simplify the demonstration, let us define:

$$A = \exp(-TR \cdot R_{10}), \tag{A.3}$$

$$B = \exp(-TR \cdot r_1 c(t)). \tag{A.4}$$

Let us define:

$$S^* = \frac{S_0}{S_{eq} \sin\alpha}, \tag{A.5}$$

$$= \frac{1 - A}{1 - A\cos\alpha}. \tag{A.6}$$

Thus,

$$S^* \frac{s(t)}{S_0} = \frac{S_0}{S_{eq} \sin\alpha} \frac{s(t)}{S_0}, \tag{A.7}$$

$$= \frac{1 - AB}{1 - AB\cos\alpha}. \tag{A.8}$$

Now, let us define:

$$\frac{1-\cos\alpha\cdot S^*\frac{s(t)}{S_0}}{1-S^*\frac{s(t)}{S_0}} = \frac{1-\cos\alpha\left(\frac{1-AB}{1-AB\cos\alpha}\right)}{1-\frac{1-AB}{1-AB\cos\alpha}}, \tag{A.9}$$

$$= \frac{1-AB\cos\alpha-\cos\alpha(1-AB)}{1-AB\cos\alpha-(1-AB)}, \tag{A.10}$$

$$= \frac{1-AB\cos\alpha-\cos\alpha+AB\cos\alpha}{1-AB\cos\alpha-1+AB}, \tag{A.11}$$

$$= \frac{1-\cos\alpha}{AB(1-\cos\alpha)}, \tag{A.12}$$

$$= \frac{1}{AB}. \tag{A.13}$$

Thus,

$$-TR\cdot R_{10}-TR\cdot r_1 c(t) = \ln\left(\frac{1-\cos\alpha\cdot S^*\frac{s(t)}{S_0}}{1-S^*\frac{s(t)}{S_0}}\right). \tag{A.14}$$

Therefore,

$$c(t) = \frac{1}{TR\cdot r_1}\ln\left(\frac{1-\cos\alpha\cdot S^*\frac{s(t)}{S_0}}{1-S^*\frac{s(t)}{S_0}}\right) - \frac{R_{10}}{r_1}. \tag{A.15}$$

References

Brix, G., Semmler, W., Port, R., Schad, L.R., Layer, G., Lorenz, W.J., 1991. Pharmacokinetic parameters in cns gd-dtpa enhanced mr imaging. Journal of computer assisted tomography 15, 621–628.

Carr, J.C., Carroll, T.J., 2011. Magnetic resonance angiography: principles and applications. Springer Science & Business Media.

Chen, J., Yao, J., Thomasson, D., 2008. Automatic determination of arterial input function for dynamic contrast enhanced mri in tumor assessment, in: International Conference on Medical Image Computing and Computer-Assisted Intervention, Springer. pp. 594–601. doi:10.1007/978-3-540-85988-8_71.

De Bazelaire, C.M., Duhamel, G.D., Rofsky, N.M., Alsop, D.C., 2004. Mr imaging relaxation times of abdominal and pelvic tissues measured in vivo at

3.0 t: preliminary results 1. Radiology 230, 652–659. doi:10.1148/radiol.2303021331.

Fennessy, F.M., Fedorov, A., Penzkofer, T., Kim, K.W., Hirsch, M.S., Vangel, M.G., Masry, P., Flood, T.A., Chang, M.C., Tempany, C.M., et al., 2015. Quantitative pharmacokinetic analysis of prostate cancer dce-mri at 3t: comparison of two arterial input functions on cancer detection with digitized whole mount histopathological validation. Magnetic resonance imaging 33, 886–894. doi:10.1016/j.mri.2015.02.008.

Ferlay, J., Shin, H.R., Bray, F., Forman, D., Mathers, C., Parkin, D.M., 2010. Estimates of worldwide burden of cancer in 2008: Globocan 2008. International journal of cancer 127, 2893–2917. doi:10.1002/ijc.25516.

Giannini, V., Mazzetti, S., Vignati, A., Russo, F., Bollito, E., Porpiglia, F., Stasi, M., Regge, D., 2015. A fully automatic computer aided diagnosis system for peripheral zone prostate cancer detection using multi-parametric magnetic resonance imaging. Computerized Medical Imaging and Graphics 46, 219–226. doi:10.1016/j.compmedimag.2015.09.001.

Gliozzi, A., Mazzetti, S., Delsanto, P.P., Regge, D., Stasi, M., 2011. Phenomenological universalities: a novel tool for the analysis of dynamic contrast enhancement in magnetic resonance imaging. Physics in medicine and biology 56, 573.

Haase, A., Frahm, J., Matthaei, D., Hanicke, W., Merboldt, K.D., 1986. Flash imaging. rapid nmr imaging using low flip-angle pulses. Journal of Magnetic Resonance (1969) 67, 258–266. doi:10.1016/0022-2364(86)90433-6.

Heilmann, M., Kiessling, F., Enderlin, M., Schad, L.R., 2006. Determination of pharmacokinetic parameters in dce mri: consequence of nonlinearity between contrast agent concentration and signal intensity. Investigative radiology 41, 536–543. doi:10.1097/01.rli.0000209607.99200.53.

Hoffmann, U., Brix, G., Knopp, M.V., Heβ, T., Lorenz, W.J., 1995. Pharmacokinetic mapping of the breast: a new method for dynamic mr mammography. Magnetic resonance in medicine 33, 506–514. doi:10.1002/mrm.1910330408.

Huisman, H.J., Engelbrecht, M.R., Barentsz, J.O., 2001. Accurate estimation of pharmacokinetic contrast-enhanced dynamic mri parameters of the prostate. Journal of Magnetic Resonance Imaging 13, 607–614. doi:10.1002/jmri.1085.

Lemaître, G., Martí, R., Freixenet, J., Vilanova, J.C., Walker, P.M., Meriaudeau, F., 2015. Computer-aided detection and diagnosis for prostate cancer based on mono and multi-parametric mri: A review. Computers in biology and medicine 60, 8–31. doi:10.1016/j.compbiomed.2015.02.009.

Meng, R., Chang, S.D., Jones, E.C., Goldenberg, S.L., Kozlowski, P., 2010. Comparison between population average and experimentally measured arterial input function in predicting biopsy results in prostate cancer. Academic radiology 17, 520–525. doi:10.1016/j.acra.2009.11.006.

Parker, G.J., Roberts, C., Macdonald, A., Buonaccorsi, G.A., Cheung, S., Buckley, D.L., Jackson, A., Watson, Y., Davies, K., Jayson, G.C., 2006. Experimentally-derived functional form for a population-averaged high-temporal-resolution arterial input function for dynamic contrast-enhanced mri. Magnetic resonance in medicine 56, 993–1000. doi:10.1002/mrm.21066.

Schabel, M.C., Parker, D.L., 2008. Uncertainty and bias in contrast concentration measurements using spoiled gradient echo pulse sequences. Physics in medicine and biology 53, 2345. doi:10.1088/0031-9155/53/9/010.

Shanbhag, D., Gupta, S.N., Rajamani, K., Zhu, Y., Mullick, R., 2012. A generalized methodology for detection of vascular input function with dynamic contrast enhanced perfusion data, in: ISMRM, p. 10.

Tofts, P.S., Berkowitz, B., Schnall, M.D., 1995. Quantitative analysis of dynamic gd-dtpa enhancement in breast tumors using a permeability model. Magnetic Resonance in Medicine 33, 564–568. doi:10.1002/mrm.1910330416.

Weinreb, J.C., Barentsz, J.O., Choyke, P.L., Cornud, F., Haider, M.A., Macura, K.J., Margolis, D., Schnall, M.D., Shtern, F., Tempany, C.M., et al., 2016. Pi-rads prostate imaging–reporting and data system: 2015, version 2. European urology 69, 16–40.

Zhu, Y., Chang, M.C., Gupta, S., 2011. Automated determination of arterial input function for dce-mri of the prostate, in: SPIE Medical Imaging, International Society for Optics and Photonics. pp. 79630W–79630W. doi:10.1117/12.878213.